Journal of Applied Polymer Science

Preparation of Nanostructured Porous Carbon Composite Fibers from Ferrum Alginate Fibers

Bingbing Wang, Qingshan Kong, Fengyu Quan, Quan Ji, Yanzhi Xia
State Key Laboratory Cultivating Base for New Fiber Materials and Modern Textile, Qingdao University, Qingdao 266071, People's Republic of China
Correspondence to: Y. Xia (E-mail: qdxyzh@163.com)

ABSTRACT: Nano-microstructured porous carbon composite fibers (Fe_2O_3@C/FeO@C/Fe@C) were synthesized by the thermal decomposition of ferrum alginate fibers. The ferrum alginate fiber precursors were prepared by wet spinning, and calcined at 300–1000°C in high purity nitrogen. The resulting composite fibers consist of carbon coated Fe_2O_3/FeO/Fe nanoparticles and porous carbon fibers. All the prepared nanostructures were investigated using thermal gravimetry, X-ray diffraction (XRD), Fourier transform infrared spectroscopy, transmission electron microscope (TEM), and nitrogen adsorption–desorption isotherm. The results show that there are five stages in the decomposition process of the ferrum alginate fibers. Transitions between the five stages are affected by the decomposition temperature. XRD results show that maghemite (Fe_2O_3), wüstite (FeO), martensite (Fe) nanoparticles were formed at 300–500°C, 600–700°C, 800–1000°C, respectively. Scanning electron microscopy and TEM results indicate that the composite fibers consist of nanoparticles and porous carbon. The diameter of the nanosized particles increased from 100 to 500 nm with increasing reaction temperature. The nitrogen adsorption–desorption results also show that the composite fibers have a micro- and mesoporous structure. © 2012 Wiley Periodicals, Inc. J. Appl. Polym. Sci. 000: 000–000, 2012

KEYWORDS: alginate; fibers; nanoparticle; porous carbon; adsorption

Received 20 May 2011; accepted 12 March 2012; published online
DOI: 10.1002/app.37679

INTRODUCTION

Biopolymers are a renewable resource with particular potential for the preparation of porous carbon materials.[1] Alginate is a rapidly developing ocean origin biopolymer, obtained from cell walls of brown algae. Alginate is composed of 1–4 linked-L-guluronic (G) and-D-mannuronic (M) acid residues and acts as a reinforcing element (similarly to cellulose in land plants) in the cell walls of brown seaweeds.[2] Alginate has been widely used in wound management,[3] controlled delivery of drugs,[4] and immobilization of enzymes and proteins.[5] There are some studies on the preparation of carbon materials from alginate.[6–8] However, few studies have been reported concerning the preparation of carbon materials from ferrum alginate fibers. Because of the polymeric carbon matrix of the alginate having abundant hydroxyl and carboxyl groups, carbonaceous materials can be converted from the polymeric carbon matrix by high temperature carbonization. When all these functional groups have been converted into carbon oxides and water at high temperature, porous carbon materials can be obtained from alginate fibers.[9] Porous carbons potentially offer an attractive and inexpensive option for the removal of organic and inorganic contaminants from water.[10,11] Their high specific surface area and porous structure means that porous carbons can efficiently adsorb gases and compounds dispersed or dissolved in liquids.[12–14] The adsorption of several organic contaminants in water, such as pesticides, phenols and chlorophenols, has recently been reported.[15–19] Moreover, porous carbon can easily be functionalized and used as an efficient adsorbent for heavy metal cationic contaminants.[20]

Over the past decades, the preparation of porous carbon materials has been centered on templating technology using mesoporous zeolites and silica as hard templates,[21,22] and polymer foams, microspheres, or amphiphilic copolymers as soft templates.[23–25] However, the above-mentioned methods are complex because of the multiple process steps and the need to remove the sacrificial templates. Various chemical and physical activating methods have been developed in which additional inorganic compounds are used as activating agents[26,27]; however, these methods are also limited by their complexity.

Wüstite (FeO) and maghemite (Fe_2O_3) nanoparticles have a wide range of potential applications. Wüstite is of great importance for catalysis in solid-state physics and chemistry. A

number of structural, magnetic, and electron transitions appeared in FeO, and its nonstoichiometric nature ($Fe_{1-x}O$, where x varies up to 0.12) significantly complicates the phase diagram.[28,29] The maghemite form of iron oxide (γ-Fe_2O_3) is a ferromagnetic oxide that is already widely used in magnetic recording materials. In addition to magnetic recording, maghemite nanoparticles are potentially useful for a number of different applications such as, magneto-optical devices,[30] magnetic refrigeration,[31] and controlled drug delivery.[32] Magnetic particles can also be used to adsorb contaminants from aqueous or gaseous effluents. The maghemite particles can be separated from the medium by a simple magnetic process after adsorption.[33–35] However, the particles have the drawback of a small surface area and, therefore, small adsorption capacity, which limits their application. In addition, the preparation of these magnetic materials requires sophisticated and costly procedures, and the use of toxic chemicals.

We have prepared ferrum alginate fibers by wet-spinning and ion exchange. High surface area and adsorption capacity magnetic composites fibers (Fe_2O_3@C/FeO@C/Fe@C) were prepared by the thermal decomposition of the ferrum alginate fibers. The obtained materials exhibit a composite structure of porous carbon and nanosized maghemite (Fe_2O_3)/wüstite (FeO)/martensite (Fe). The Fe_2O_3/FeO/Fe nanoparticles were prepared by calcining at 300–500°C, 600–700°C, 800–1000°C, respectively. The composites fibers can be used for the removal of contaminants from aqueous effluents.

The spinning process for alginate fibers is environmentally friendly, using no toxic or organic solvents. The use of cation exchange enables many kinds of alginate fibers to be prepared.[36,37] Generally, alginate gelation takes place when divalent cations (e.g., Ca^{2+}) interact ionically with blocks of guluronic acid residues, resulting in formation of a firm chelation network which is usually described by the "egg-box" model. However, it is difficult to produce alginate fibers with trivalent cations (e.g., Fe^{3+}, Al^{3+}),[36] because the trivalent cations are expected to form a three-dimensional valent bonding structure with the sodium alginate. The crosslinking occurs in two different planes at the same time, resulting in compaction of the alginate molecules. Therefore, the trivalent cations crosslinked beads tend to be brittle.[36] Therefore, we prepared our ferrum alginate fibers by ion exchange. Calcium alginate fibers were prepared by wet spinning. Then, Ferrum alginate fibers were prepared by the ionic exchange of Fe^{3+} in $FeCl_3$ solution and Ca^{2+} in the calcium alginate fibers. The porous composite materials were then synthesized by high-temperature treatment of the wet-spun ferrum alginate fibers in a N_2 gas stream. Neither sophisticated techniques nor metal catalysts are used in this approach. We also report on the adsorption performance and behavior of the porous carbon.

EXPERIMENTAL

Materials

High viscosity alginate sodium salt (120 mPa s) was supplied by the Qingdao Mingyue Company. Calcium chloride (analytical grade) was supplied by the Tianjin Guangcheng Company. Ferrum chloride (analytical grade) was supplied by the Tianjin Bodi Company.

Methods

The calcium alginate fibers were prepared by wet spinning, based on the exchange of sodium ions in alginate and divalent cations in a coagulating bath. The spinning equipment was built basing on our own design. A 5.0% aqueous spinning solution of sodium alginate was vigorously stirred at room temperature for an hour. The solution was filtered through a 200-mesh filter cloth under pressure and degassed in the spinning tank. The filtered solution was extruded through a 30-hole (0.08 mm in diameter) viscose-type spinneret into a coagulating bath containing 4.5 wt % $CaCl_2$ at 25°C. The coagulating bath contained aqueous calcium chloride. The as-spun fibers were washed and stretched with a stretching ratio of 20% in distilled water and dried (The flow chart is shown in Figure 1). The generated fibers were put in 5 wt % ferrum chloride solution for ionic exchange. The obtained ferrum alginate fibers were dried in a drying oven at 60°C for 24 h.

The high-temperature treatment of the ferrum alginate fibers was performed in a single zone tube furnace (OTF-1200X). The as-prepared nanostructured composite fibers (Fe_2O_3@C/FeO@C/Fe@C) were prepared by thermal decomposition of the obtained ferrum alginate fibers in high purity N_2 at 200–1000°C in increments of 100°C. The heating rate was 10 K/min. The time maintained at the target temperature was 10 h. The fibers were then cooled to room temperature.

Characterization

The mechanical properties of the fibers were measured according to standard ISO5079:1999 using a Favimat-airobot single fiber testing machine (Textechno Company). The initial sample length was 15.0 mm and stretching rate was 20.0 mm/min. The samples were tested fifty times. The force at the breaking point was measured as tensile stress from which the tensile strength was calculated. Variations in the elemental concentrations in the fibers caused by ionic exchange of Ca^{2+} and Fe^{3+} were measured using inductively coupled plasma atomic emission spectroscopy (ICP) using a PerkinElmer Optima 2100DV instrument. IR spectra were recorded using a Thermo NICOLET 5700 system with a resolution of 8 cm^{-1}, using KBr tablets to contain the alginate fibers. Scanning electron microscopy (SEM) images were collected on a JSM-6390LV scanning electron microscope. Particle size and morphology of the as-obtained products were investigated by transmission electron microscopy (TEM, JEM-1200EX). Thermogravimetric analysis (TGA) was done using a TA Q500 thermogravimetric analyzer at a scanning rate of 10°C/min under N_2, from room temperature to 1000°C. X-ray diffraction (XRD) patterns of the films were investigated using a D8 Advance X-ray diffractometer with CuK-α_1 radiation. Adsorption isotherms for N_2 at 77 K were determined using a Micromeritics TriStar 3000 surface area analyzer. Surface areas were determined using the Brunauer–Emmett–Teller (BET) method. Pore size distributions were determined by the Barrett–Joyner–Halenda (BJH) method applied to desorption branch of the N_2 isotherm. The microporous surface (Smicro) and external surface (Sext), as well as

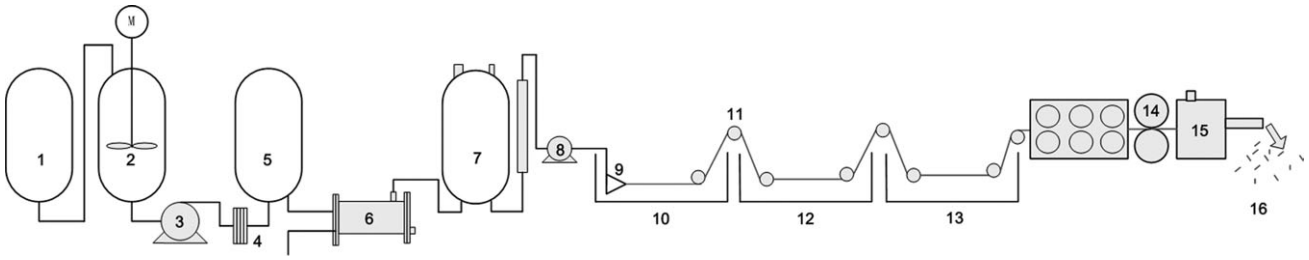

Figure 1. The process of wet spinning of alginate fibers (1. predissolving; 2. dissolving kettle; 3. wheel pump; 4. frame filter; 5. accumulator still; 6. kk-filter; 7. deaeration kettle; 8. metering pump; 9. spinneret; 10. coagulation; 11. filament roller; 12. washing bath; 13. stretching/crosslinking bath; 14. convolution roller; 15. fiber cutting/drying; 16. short fibers). [Color figure can be viewed in the online issue, which is available at wileyonlinelibrary.com.]

the micropore volume (Vmi) were evaluated by the t-plot method, and mesopore volume (Vme) was estimated by the BJH method. The total pore volume was evaluated by summation of microporous and mesoporous volumes.

RESULTS AND DISCUSSION

Mechanical Properties of Fibers

The tensile strength of the fibers is shown in Table I. The tensile strength of the calcium alginate fibers (26.12) was higher than that of ferrum alginate fibers (21.33). The decrease in tensile strength of the ferrum alginate fibers may be explained by chelation between Fe^{3+} and —OH in the alginate. Radius and valence of Ca^{2+} and Fe^{3+} are different, so as crosslinking occurs, there is a three-dimensional bonding structure formed between alginate and Fe^{3+}. This bonding structure occurs simultaneously in two different planes, and thus differs from the in-plane chelation of Ca^{2+} and —OH.[36] The tensile strength of the calcined fibers is close to nil, which may be attributed to the dense nano-micro holes in the obtained fibers.

As shown in Table I, the breaking elongation and linear density of the calcium alginate fibers were lower than ferrum alginate fibers. The increase in breaking elongation and linear density of the ferrum alginate fibers can be explained by the three-dimensional crosslinking formed between alginate and Fe^{3+}. The crosslinking occurs simultaneously in two different planes resulting in compaction of the alginate molecules (Figure 3). The relative motion of the alginate molecules is limited, giving an increase in breaking elongation and linear density.

Table I. Tensile Properties of Alginate Fibers

Material		Tensile strength (cN/tex)	Breaking elongation (%)	Linear density (dtex)
Calcium fiber	Test results	26.1	3.4	5.3
	Variation coefficient (%)	12.5	11.6	8.7
Ferrum fiber	Test results	21.3	4.1	5.6
	Variation coefficient (%)	15.7	14.8	13.8

Fourier Transform Infrared Spectroscopy

Figure 2 shows the IR spectra of sodium alginate (a), calcium alginate fibers (b), and ferrum alginate fibers (c). In curve (a), the vibrational bands at 3446 and 2927 cm^{-1} are assigned to —OH and —CH stretching vibrations, the band at 1417 cm^{-1} is assigned to —CH flexural vibration, the band between 1034 and 1095 cm^{-1} arises from the C—O—C stretching vibration, and the band at 1619 cm^{-1} is assigned to —COOH stretching vibration.

After crosslinking with Ca^{2+} [Figure 2(b)] or Fe^{3+} [Figure 2(c)], the —OH stretching vibration at 3449 cm^{-1} becomes sharper, and the C—O—C stretching vibration becomes weaker. This indicates the existence of chelation between Ca^{2+} (or Fe^{3+}) and —OH. The chelation limits the C—O—C stretching vibration. The strong peak at 1596 cm^{-1} for the —COOH stretching vibration is shown in curve (c). This spectral change results from a three-dimensional valent bonding structure between sodium alginate and Fe^{3+}. The reason being that crosslinking occurs simultaneously in two different planes, differing from the in-plane chelation of Ca^{2+} and —OH, which is usually described by the "egg-box" model[36] (Figure 3). This result is in accord with the measurements of the tensile strength of the fibers.

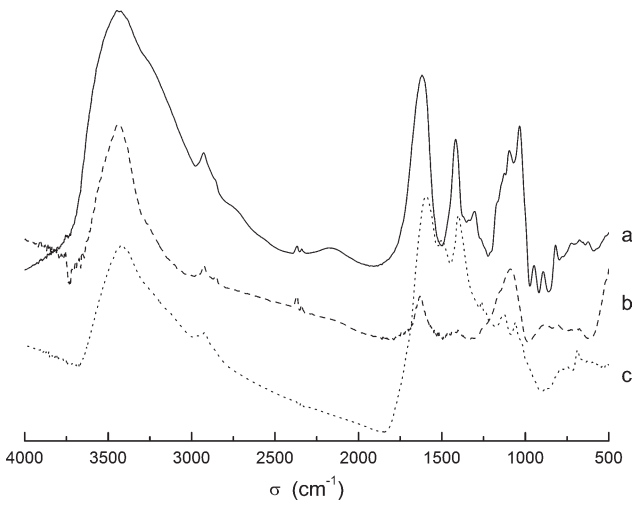

Figure 2. FTIR of (a) sodium alginate; (b) calcium alginate fibers; (c) ferrum alginate fibers.

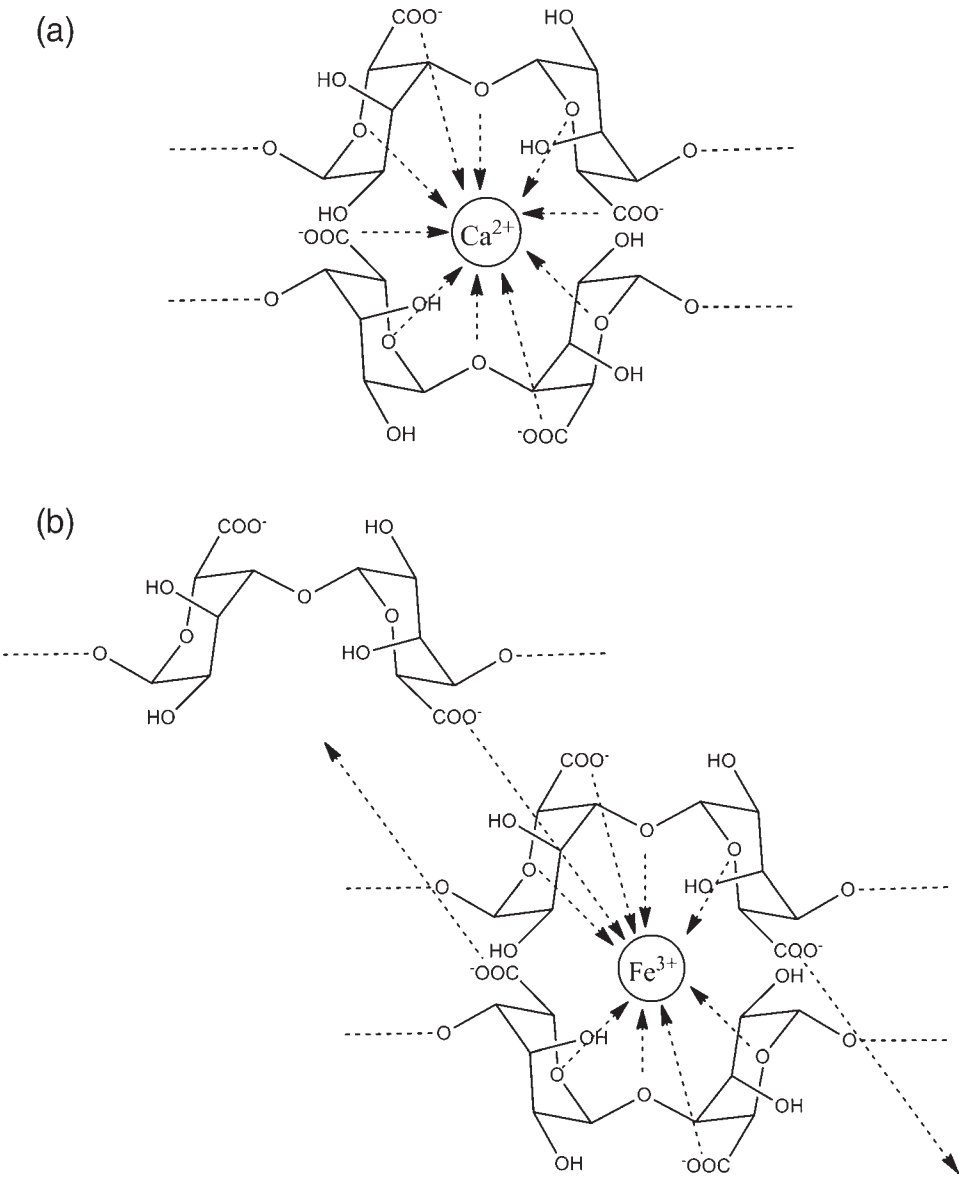

Figure 3. Chelation of (a) Ca-alginate and (b) Fe-alginate.

Inductively Coupled Plasma Atomic Emission Spectroscopy

Table II shows variations in the calcium and ferrum concentrations of the fibers caused by ion exchange between the calcium alginate fibers and the $FeCl_3$ aqueous solution. It can be seen from Table I that fibers treated with $FeCl_3$ solution show a significant decrease of about 99.84% in the Ca^{2+} concentration and a significant increase in the Fe^{3+} concentration.

The results indicate that the fibers treated with $FeCl_3$ solution do exchange calcium ions in the fibers with the ferrum ions in the $FeCl_3$ solution. Considering also the IR spectra of the fibers, there is an indication that there is chelate structure between Fe^{3+} and alginate in the ion exchanged fibers.

Thermogravimetric Analysis

Ferrum alginate fibers were heated to 1000°C in a tube furnace with heating rate of 10°C/min in N_2 and kept at 1000°C for 2 h. This treatment is similar to the high-temperature treatment of certain divalent metal alginate gel compounds.[38] The weight loss up to 210°C corresponds to the loss of water of hydration. Then from 200 to 300°C, the curve indicates the degradation of ferrum alginate with the rupture of bonds to form an intermediate compound. It is the decomposition of this intermediate fragment that gives the corresponding ferrum oxide (Figure 4). Consequently, the decomposition of the ferrum alginate complexes can be divided into five stages with the suggested mechanisms described by these equations:

$$(C_{12}H_{14}O_{11})_3Fe_2XH_2O \xrightarrow{\text{up to } 200^\circ C} (C_{12}H_{14}O_{11})_3Fe_2 + XH_2O \quad (1)$$

$$(C_{12}H_{14}O_{11})_3\,Fe_2 \xrightarrow{200-300^\circ C} 2\,Fe(COO)_3 + 30C + 21H_2O \quad (2)$$

Table II. The Elemental Concentrations Variations of (a) Calcium Alginate Fibers and (b) Fibers with Ion Exchanged between Ca^{2+} and Fe^{3+}

Sample	Symbol	Wavelength (nm)	Sample flow rate (mL/min)	Sample conc. units (mg/L)	Weight (mg)	Ion content (%)	Exchange ratio (%)
a	Ca	317.993	1.5	86.365	103.9	8.31	
	Fe	238.204	1.5	0.138	103.9	0.013	
b	Ca	317.993	1.5	0.141	109.3	0.013	−99.8401
	Fe	238.204	1.5	147.7	109.3	13.51	99.9999

$$Fe(COO)_3 \xrightarrow{300-400^\circ C} Fe_2O_3 + CO_2 \quad (3)$$

$$Fe_2O_3 + C \xrightarrow{600-800^\circ C} FeO + CO_2 \quad (4)$$

$$FeO + C \xrightarrow{800^\circ C} C_{0.055}Fe + CO_2 \quad (5)$$

X-ray Diffraction

Figure 5 shows the XRD patterns of the samples thermal degraded at 300–900°C. All the diffraction peaks in Figure 5(a–c) are in good agreement with Maghemite (Fe_2O_3) [PDF No.25-1402]. The diffraction peaks of (220), (311), (400), (00 12), (511), (440), and (533) are shifted to higher intensities with the rise of the thermal degradation temperature. No other peaks are observed, indicating the high purity of the as-prepared Fe_2O_3, which is in accordance with the above mechanism. The wüstite (FeO) particles, as shown in Figure 5(d–e), were collected at 600–700°C. The diffraction peaks observed can be indexed to the (111), (110), (121), and (020) planes of wüstite (FeO) [PDF No.85-0625]. Figure 5(f,g) shows the XRD patterns of samples with thermal treatment at 800–900°C. All of the peaks can be indexed to the (101), (110), and (200) planes of Martensite ($C_{0.055}$ $Fe_{1.945}$), consistent with [PDF No.44-1290]. These peaks may be attributed to the two successive electrochemical processes shown in eqs. (4) and (5).

Scanning Electron Microscopy

To understand the formation process of the Fe_2O_3/FeO nanostructures and the porous carbon, we carried out further studies of the samples collected at different temperatures. As shown in Figure 6(a,d), the cross-section of the fibers is circular and the surface is smooth. This may be due to the fact that in the spinning process, the fibers undergo quick and high permeation of solvent which results in uniform coagulation. However, the irregular and toothed shape in Figure 6 may be caused by the coagulation of the sodium alginate solution that takes place first on the surface and then further delayed coagulation in the interior during the spinning process. As shown in Figure 6(a), the ferrum alginate fibers have smooth surface with an average diameter of about 10 μm. There are no particles on the surface of the fibers nor on the fibers calcined at 200°C [Figure 6(b)]. The diameter of the calcined fibers is about 10 μm [Figure 6(c,d)]. Figure 6(c) shows the SEM image of a typical sample with thermal treatment at 300°C. The product is composed of many rhombohedral nano- or microstructured particles, ~ 100 nm in diameter, which distribute among the surface of the fibers. The sample collected from 400 to 500°C showed that the diameter change from 100 to 500 nm occurs between 400 and 500°C [Figure 6(d)].

As the reaction temperature is increased, uniform spheres are formed between 600 and 1000°C. As shown in Figure 6(e,f), the nanoparticles congregate together and melt into larger diameter particles, decreasing the number of particles. In this formation process, temperature is found to be the key controlling factor. Pores are uniformly dispersed in the carbon fibers. These images are in accordance with the proposed five successive processes described by eqs. (1)–(5).

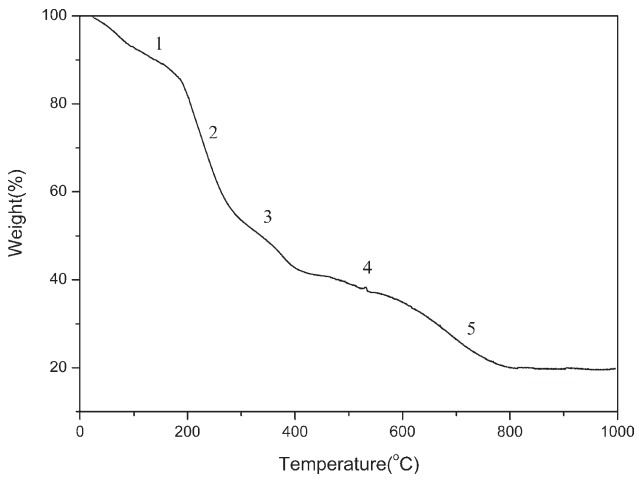

Figure 4. TG curve of ferrum alginate fibers in N_2 atmosphere.

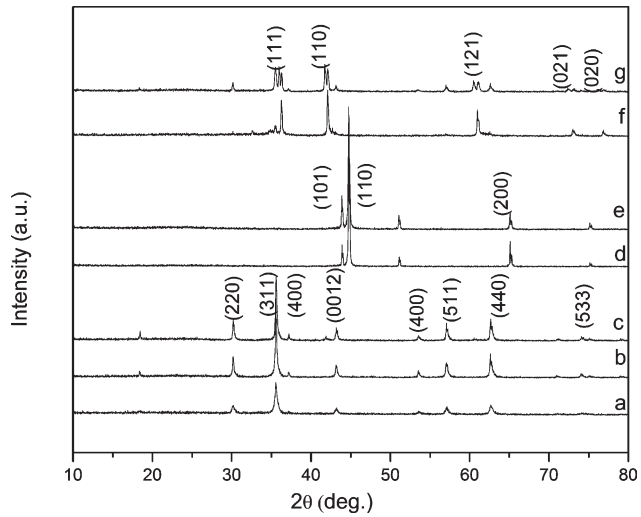

Figure 5. XRD patterns of structures with thermal degradations at (a) 300°C; (b) 400°C; (c) 500°C; (d) 600°C; (e) 700°C; (f) 800°C; and (g) 900°C.

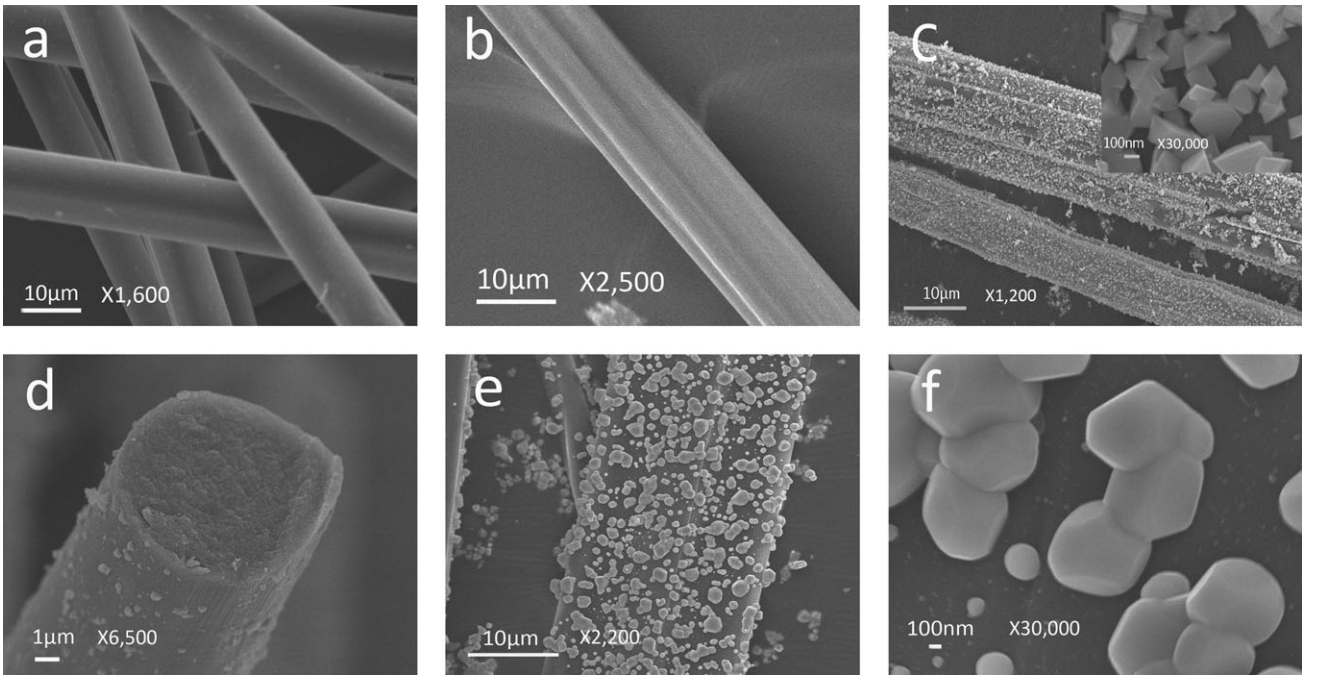

Figure 6. SEM images of (a) ferrum alginate fibers without treatment; (b) surface of ferrum alginate fibers with calcination at 200°C; (c) 300°C; (d) 400°C; (e, f) 700°C

Transmission Electron Microscopy

TEM analysis was used to further examine the morphology of the as-prepared fibers collected at 400°C (Figure 7). TEM images showing uniform sized Fe_2O_3 particles are shown in Figure 7(a). The average size of the Fe_2O_3 particles is 50 nm in diameter, 100–150 nm in length. Figure 7(b) shows the morphology of ground porous carbon. The existence of the accumulated carbon in Section I may be ascribed to the existence of a squeezed hierarchical structure. The TEM image in Section II is typical spread carbon. It can be seen that the sample is comprised of uniform sized Fe_2O_3 nanoparticles and nanoscale carbon. The results give a further indication that the images in

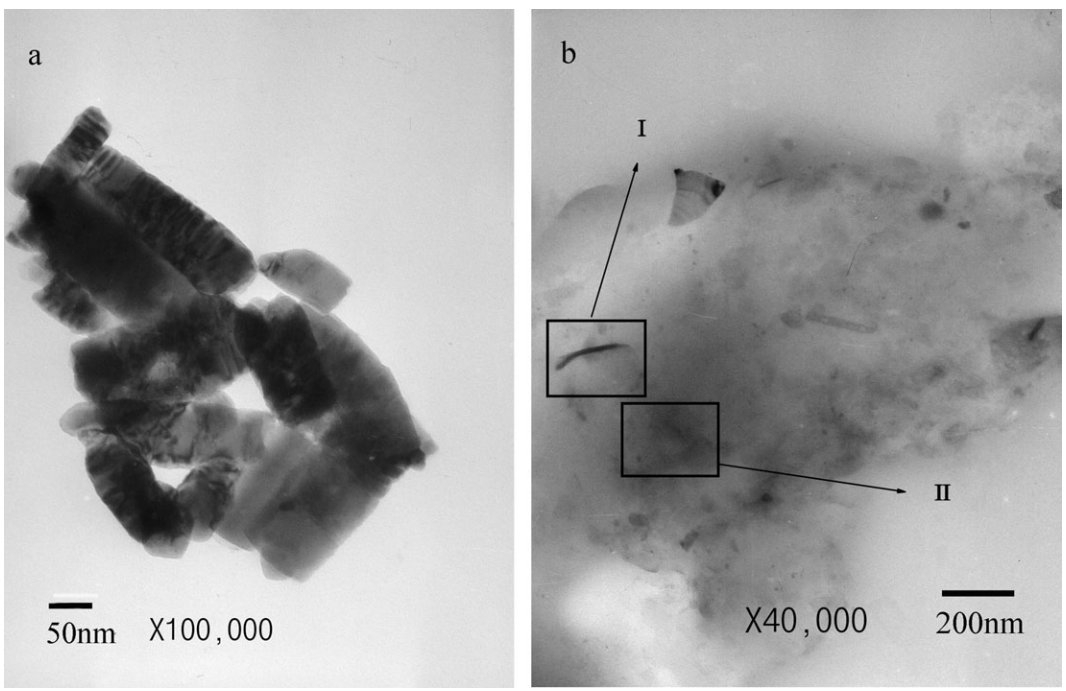

Figure 7. TEM image of composite material with thermal treatment at 400°C: (a) Fe_2O_3 particles; (b) porous carbon grinded in a mortar (I: accumulated hierarchical carbon; II: spreaded hierarchical carbon).

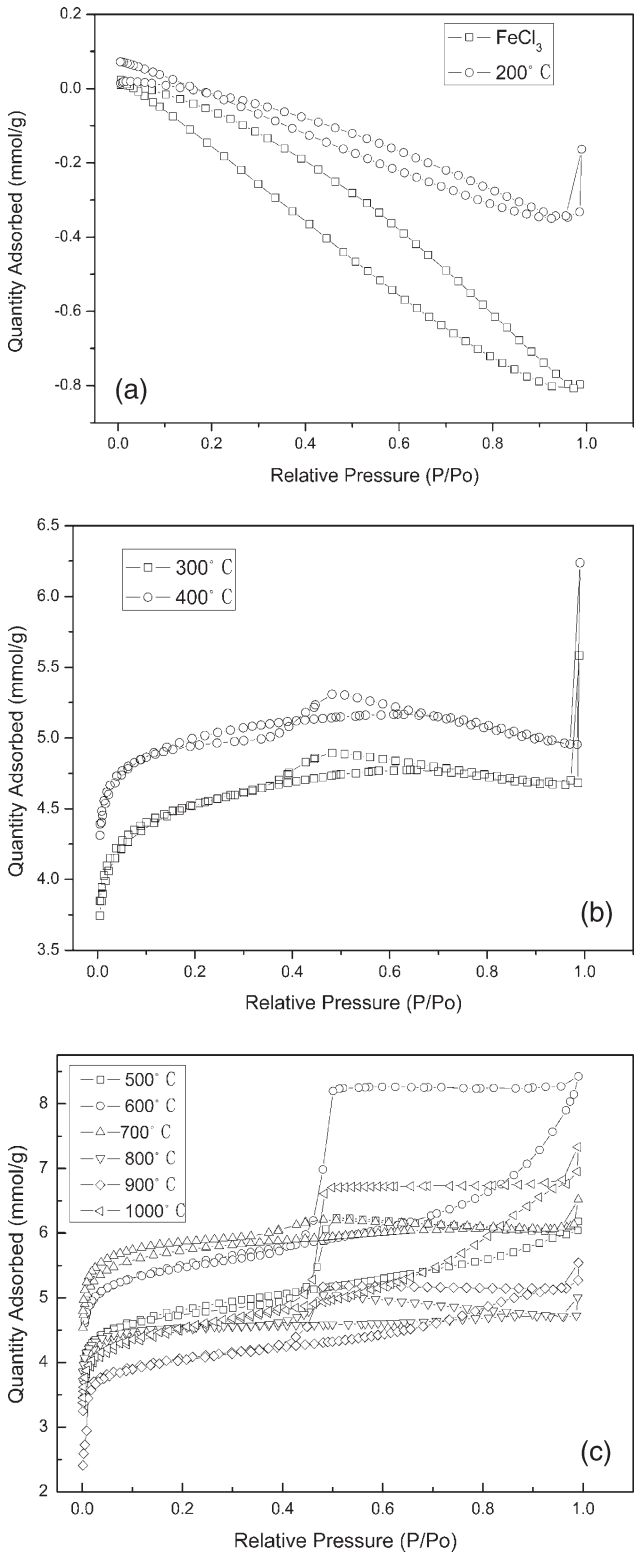

Figure 8. (a) Nitrogen adsorption/desorption isotherms on Fe-alg fibers and the fibers with thermal treatment at 200°C. (b) Nitrogen adsorption/desorption isotherms on Fe-alg fibers with thermal treatment at 300°C and 400°C. (c) Nitrogen adsorption/desorption isotherms on Fe-alg fibers with thermal treatment at 500–1000°C.

Figures 6 and 7 are in accordance with the proposed five-stage mechanism.

Adsorption Experiments

Further work was carried out to investigate the details of the growth mechanism of the particles and the porosity of the looser internal structured carbon. Compared with the compact carbon structure collected at 200°C, the samples collected above 300°C have a porous carbon structure with a larger specific area. The increment of temperature may increase porosity of the fibers and may eventually result in a looser internal structure of the carbon.

The nitrogen adsorption–desorption isotherms of the high-heat treated ferrum alginate fibers are shown in Figure 8. The adsorption isotherm of ferrum alginate fibers calcined at 200°C and the isotherm without thermal degradation [Figure 8(a)] belong to no particular type in the IUPAC classification. The results are in accordance with stage 1 in Figure 4 and eqs. (1) and (2). It is obvious that there is no micropore in the sample. The isotherms at 300°C and 400°C [Figure 8(b)] belong to type I, characteristic of microporous materials. However, the samples with thermal treatment at temperatures above 500°C [Figure 8(c)] belong to type IV accompanied by H2 type hysteresis loop with steep adsorption/desorption steps. The knee of the isotherms is wide, no clear plateau is attained, and a certain hysteresis slope can be observed at intermediate and high relative pressures, indicating the presence of large micropores and mesopores (type IV). This is shown by the average pore diameter values, Dp varying between 2.03 and 2.9 nm. Note that for all isotherms [Figure 8(c)], adsorption and desorption lines overlap completely in the low relative pressure range ($P/P_0 < 0.5$), while the hysteresis loop exists in the high relative pressure region ($P/P_0 > 0.5$), which is mainly due to the presence of "ink-bottle" type pores. The ink-bottle pores have a larger pore size in the bottle body, which results in the occurrence of hysteresis in the relative high pressure region.[39] The adsorption experiments results are in accordance with the proposed five-step mechanism.

CONCLUSIONS

Nano- and microstructured Fe_2O_3/FeO porous carbon composite fibers were successfully synthesized by thermal decomposition of wet-spun ferrum alginate fibers at 300–1000°C. It was observed that the composite fibers are composed of nano particles composed with diameters of 50–500 nm and pores with narrow pore size distribution centered at 2.0–2.9 nm. The size of the particles became larger with increased reaction temperature. The specific surface areas achieved are in the range of 298–418 m^2/g. TGA, XRD, and N_2-Adsorption show that there are five stages in the decomposition process of ferrum alginate fibers. The as-prepared maghemite (Fe_2O_3), wüstite (FeO), and martensite (Fe) nanoparticles were obtained at 300–500°C, 600–700°C, 800–1000°C, respectively.

ACKNOWLEDGMENTS

We acknowledge the financial support from National Natural Science Foundation of China (No.50908120), Shandong Doctor Research Foundation (No.BS2009CL044) and Program for Taishan Scholars and Innovative Research Team.

REFERENCES

1. Hu, B.; Wang, K.; Wu, L.; Yu, S. H.; Antonietti, M.; Titirici, M. M. *Adv. Mater.* **2010,** *22*, 813.
2. Miraftab, M.; Qiao, Q.; Kennedy, J. F.; Anand, S. C.; Groocock, M. R. *Carbohydr. Polym.* **2003,** *53*, 225.
3. Qin, Y. M. *Polym. Adv. Technol.* **2008,** *19*, 6.
4. Sriamornsak, P.; Thirawong, N.; Korkerd, K. *Eur. J. Pharm. Biopharm.* **2007,** *66*, 435.
5. Zhou, Y.; Kajiyama, S. i.; Itoh, K.; Tanino, T.; Fukuda, N.; Tanaka, T.; Kondo, A.; Fukui, K. *Appl. Microbiol. Biotechnol.* **2009,** *84*, 375.
6. Raymundo-Piñero, E.; Leroux, F.; Béguin, F. *Adv. Mater.* **2006,** *18*, 1877.
7. Raymundo-Piñero, E.; Cadek, M.; Béguin, F. *Adv. Funct. Mater.* **2009,** *19*, 1032.
8. Peng, Y. T.; Chen, Z.; Wen, J.; Xiao, Q. F.; Weng, D.; He, S. Y.; Geng H. B.; Lu, Y. F. *Nano. Res.* **2011,** *4*, 216.
9. Wu, X. L.; Chen, L. L.; Xin, S.; Yin, Y. X.; Guo, Y. G.; Kong, Q. S.; Xia, Y. Z. *Chem. Sus. Chem.* **2010,** *3*, 703.
10. Pignon, H.; Brasquet, C.; La Cloirec, P. *Water Sci. Technol.* **2000,** *42*, 355.
11. Lua, A. C.; Guo, J. *J. Environ. Eng. ASCE* **2001,** *127*, 889.
12. Culp, G. L.; Culp, R. L. New Concepts in Water Purification; Reinhold: New York, **1974.**
13. Matson, P.; Mark, H. B. Activated Carbon: Surface Chemistry and Adsorption from Solution; Dekker: New York, **1971.**
14. Ruthven, D. M. Principles of Adsorption and Adsorption Processes; Wiley: New York, **1984.**
15. Garner, I. A.; Watson-Craik, I. A.; Kirkwood, R. *J. Chem. Technol. Biotechnol.* **2001,** *76*, 932.
16. Jung, M. W.; Ahn, K. H.; Lee, Y.; Kim, K. P.; Rhee, J. S. *Microchem. J.* **2001,** *70*, 123.
17. Denizli, A.; Özkan, G.; Uçar, M. *Sep. Purif. Technol.* **2001,** *24*, 255.
18. Aksu, Z.; Yener, J. *Waste Manage.* **2001,** *21*, 695.
19. Daifullah, A. A. M.; Girgis, B. S. *Water Res.* **1998,** *32*, 1169.
20. Shim, J. W.; Park, S. J.; Ryu, S. K. *Carbon* **2001,** *39*, 1635.
21. Barata-Rodrigues, P. M.; Mays, T. J.; Moggridge, G. D. *Carbon* **2003,** *41*, 2231.
22. Gadiou, R.; Didion, A.; Gearba, R. I.; Ivanov, D. A.; Czekaj, I.; KÖtz, R.; Vix-Guterl, C. *J. Phys. Chem. Solids* **2008,** *69*, 1808.
23. Go'rka, J.; Jaroniec, M. *J. Phys. Chem. C* **2008,** *112*, 11657.
24. Xue, C.; Tu, B.; Zhao, D. *Adv. Funct. Mater.* **2008,** *18*, 3914.
25. Yang, M.; Wang, G. C. *Colloids Surf. A.* **2009,** *345*, 121.
26. Sepehri, S.; García, B. B.; Zhang, Q.; Cao, G. *Carbon* **2009,** *47*, 1436.
27. Xing, W.; Huang, C. C.; Zhuo, S. P.; Yuan, X.; Wang, G. Q.; Hulicova-Jurcakova, D.; Yan, Z. F.; Lu, G. Q. *Carbon* **2009,** *47*, 1715.
28. Pasternak, M. P.; Taylor, R. D.; Jeanloz, R.; Li, X.; Nguyen, J. H.; McCammon, C. A. *Phys. Rev. Lett.* **1997,** *79*, 5046.
29. Willis, B. T. M.; Rooksby, H. P. *Acta Cryst.* **1953,** *6*, 827.
30. Ennas, G.; Marongiu, G.; Musinu, A.; Falqui, A.; Ballirano, P.; Caminiti, R. *Mater. Res.* **1999,** *14*, 1570.
31. McMichael, R. D.; Shull, R. D.; Swartzendruber, L. J.; Bennett, L. H.; Watson, R. E. *J. Magn. Magn. Mater.* **1982,** *111*, 29.
32. Bhatnagar, S. P.; Rosensweig, R. E. *J. Magn. Magn. Mater.* **1995,** *149*, 198.
33. Kroll, E.; Winnik, F. M.; Ziolo, R. *Chem. Mater.* **1996,** *8*, 1594.
34. Tronc, F.; Prene, P.; Jolivet, J. P.; d'Orazio, F.; Lucari, F.; Fioram, D.; Godinho, M., Cherkaoui, R.; Nogues, M.; Dormann, J. L. *Hyperfine Interact.* **1995,** *95*, 129.
35. Linderoth, S.; Hendriksen, P.; Bodker, F.; Wells, S.; Davies, K.; Charles, S. W.; Morup, S. *J. Appl. Phys.* **1994,** *75*, 6583.
36. Bajpai, S. K.; Sharma, S. *React. Funct. Polym.* **2004,** *59*, 129.
37. Kakita, H.; Kamishima, H. *J. Appl. Phycol.* **2008,** *20*, 543.
38. Said, A. A.; Hassan, R. M. *Polym. Degrad. Stab.* **1993,** *39*, 393.
39. Juang, R. S.; Wu, F. C.; Tseng, R. L. *Colloids Surf. A* **2002,** *201*, 191.